Supplementary Information

Synthesis and characterization of the ultra-thin BiOCl/MXene heterostructure, for the detection of NO_2 at room temperature with enhanced moisture resistance

Jiahui Fan[a], Jun Gao[c], He Lv[a], Lin Jiang[a], Fangjie Qin[a], Yihe Fan[a], Baihe Sun[a], Jue Wang[a], Muhammad Ikram[b*], Keying Shi[a*]

a.Key Laboratory of Functional Inorganic Material Chemistry, Ministry of Education. School of Chemistry and Material Science, Heilongjiang University, Harbin, 150080, P. R. China.

b.Institute for Advanced Study, Shenzhen University, Shenzhen 518060, P. R. China.

c.Harbin Normal University, Harbin, 150025, P. R. China.

* Corresponding author

Corresponding author: Tel: +86 451 86609141; +86 451 86604920

E-mail: ikram2888@yahoo.com

E-mail: shikeying2008@163.com

Fax: +86 4518667 3647; Tel: +86 451 8660 9141

Table S1 Comparison of gas sensing performance of the previous Bi-based gas sensors with the present BiOCl/Mxene sensor.

Sensor material	Gas	Operating temperature	Gas concentration	Response (S)	Response time	Recovery time	Detection limit	Ref.
Au/BiOCl	CO_x	200-300°C	100-400pm	63.2%①	9s	-	100ppm	1
BiOCl	CO	300-400°C	800ppm	90%①	4.3s	-	100ppm	2
BiOCl	Ethanol	180°C	1000ppm	30%①	-	-	5ppm	3
Bi@CdO	Formaldehyde	130°C	100ppm	86.2%①	78s	89s	-	4
Bi^{3+}@Bi-Co	NO_2	230°C	200ppm	34%①	31s	29s	25ppm	5
Bi@In_2O_3	Acetone	200°C	1ppm	6.38	15s	35s	0.3ppm	6
Bi@SnO_2	Ethanol	300°C	100ppm	71%①	12s	30s	-	7
Bi@Zn_2SnO_4/SnO_2	Formaldehyde	180°C	50ppm	23.2%①	16s	9s	-	8
$BiFeO_3$	CO	350°C	30ppm	2.12②	25s	13s	-	9
Bi@SnO_2/rGO	Benzene	150°C	5ppm	48.6②	9s	13s	1ppm	10
BiOCl/MXene	NO_2	RT	100ppm	34.58②	3.15s	31.05s	0.03ppm	**This Work**

①: S=|Ra–Rg|/Ra×100% or S=|Rg–Ra|/Ra×100%

②: S=Ra/Rg

Table S2 Comparative response of the sensors to BiOCl/Mxene at different RH (%) (Humidity).

Sensor material	Gas	Operating temperature	Gas concentration	Response (S)	RH (%)	Ref.
Bi-SnO_2	NO	75℃	5ppm	85②	85	11
Bi_2O_3-SnO_2	NO_2	RT	2ppm	61.1%①	87.8	12
In2O3-ZnO	NO_2	RT	500ppb	3.5②	80	13
2H-MoS_2/MXene	NO_2	RT	100ppm	75%①	78	14
V_2CT_x MXene	NO_2	RT	20ppm	76%①	51.9	15
Ag_2Te	NO_2	RT	5ppm	10.2%①	90	16
Au-RGOH	NO_2	RT	0.5ppm	9%①	82	17
ZnO	NO_2	49℃	3ppm	5②	90	18
In_2O_3/ZnO	NO_2	RT	1ppm	2.5②	90	19
$Ti_3C_2T_x$/γ-PGA	NO_2	RT	50 ppm	1344%①	50	20
WO_3/$Ti_3C_2T_x$	NO_2	RT	200 ppb	145%①	99	21
$Ti_3C_2T_x$–ZnO	NO_2	RT	20 ppm	202.26①	80	22
Pt SA-$Ti_3C_2T_x$	TEA	RT	2 ppm	175%①	80	23
BQ/$Ti_3C_2T_x$	NO_2	RT	1 ppm	30%①	80	24
Ag2-$Ti_3C_2T_x$	H_2S	RT	1 ppm	51.5%①	80	25
BiOCl/MXene	NO_2	RT	100ppm	2274%① 30.54②	80	**This Work**
BiOCl/MXene	NO_2	RT	30ppb	12.9%① 1.13②	80	**This Work**

①: S=|Ra–Rg|/Ra×100% or S=|Rg–Ra|/Ra×100%

②: S=Ra/Rg

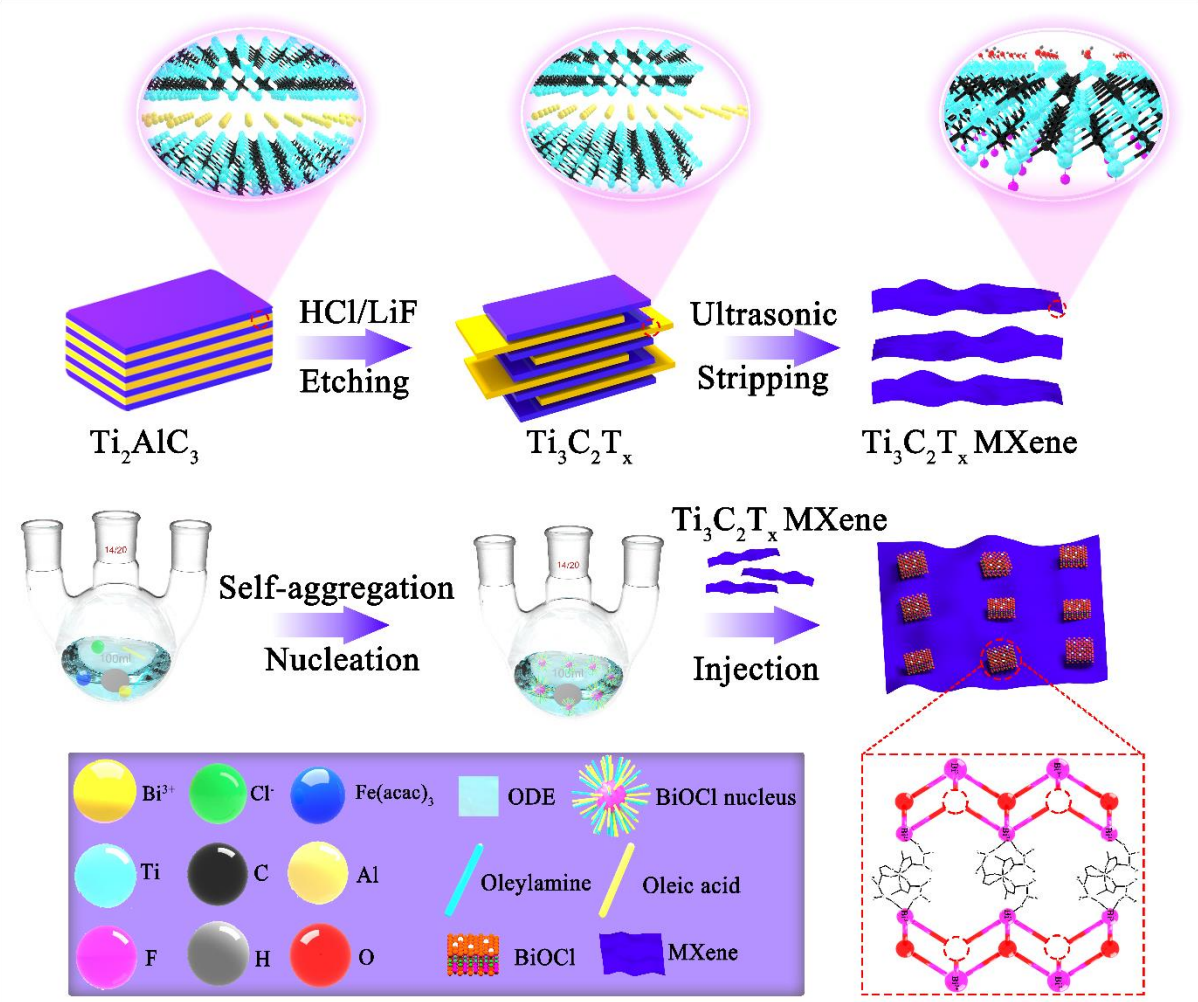

Scheme. S1. Schematic illustration for the synthesis of BiOCl/MXene composites.

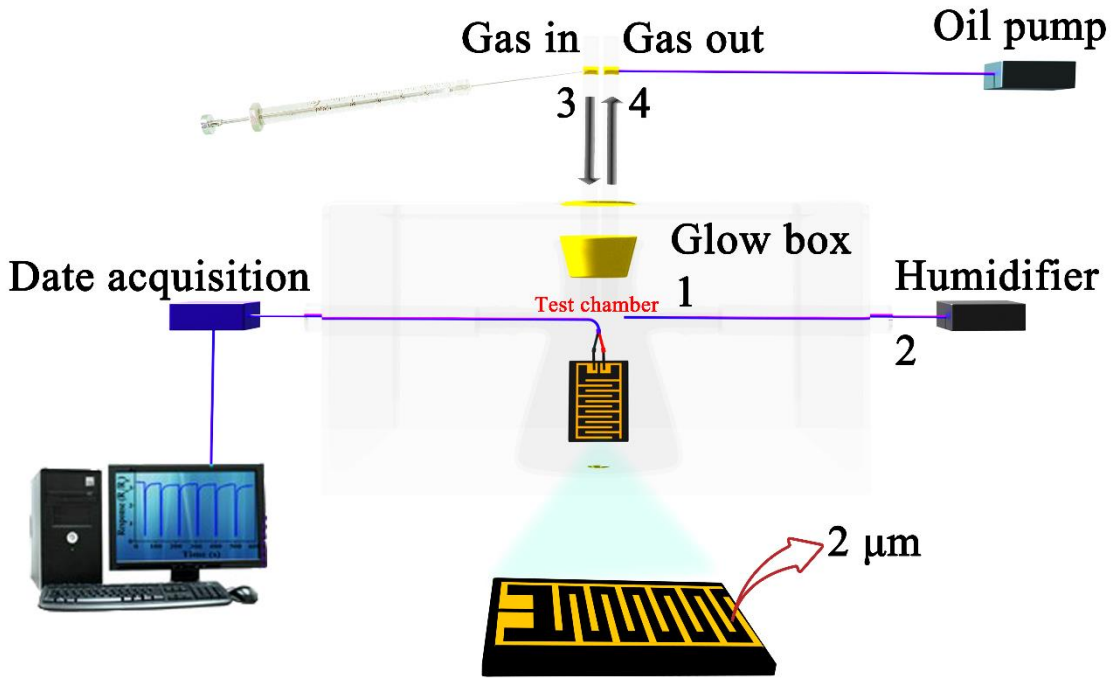

Scheme. S2. The gas delivery system diagram for the sensing process.

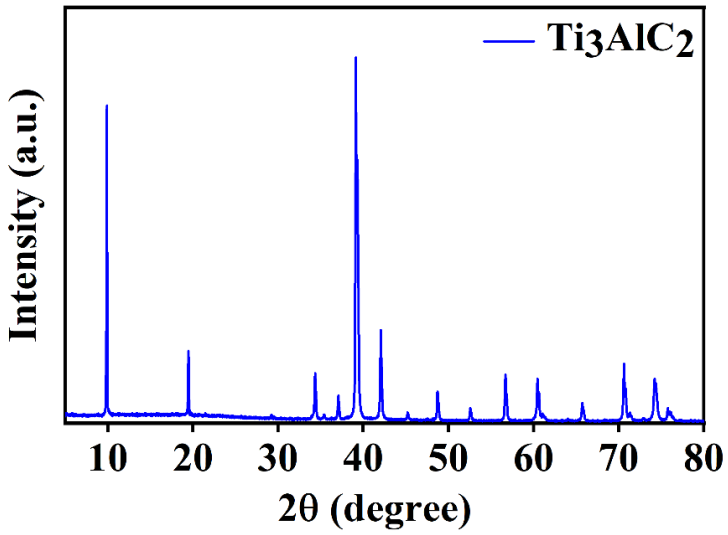

Fig. S1. XRD image of Ti_3AlC_2.

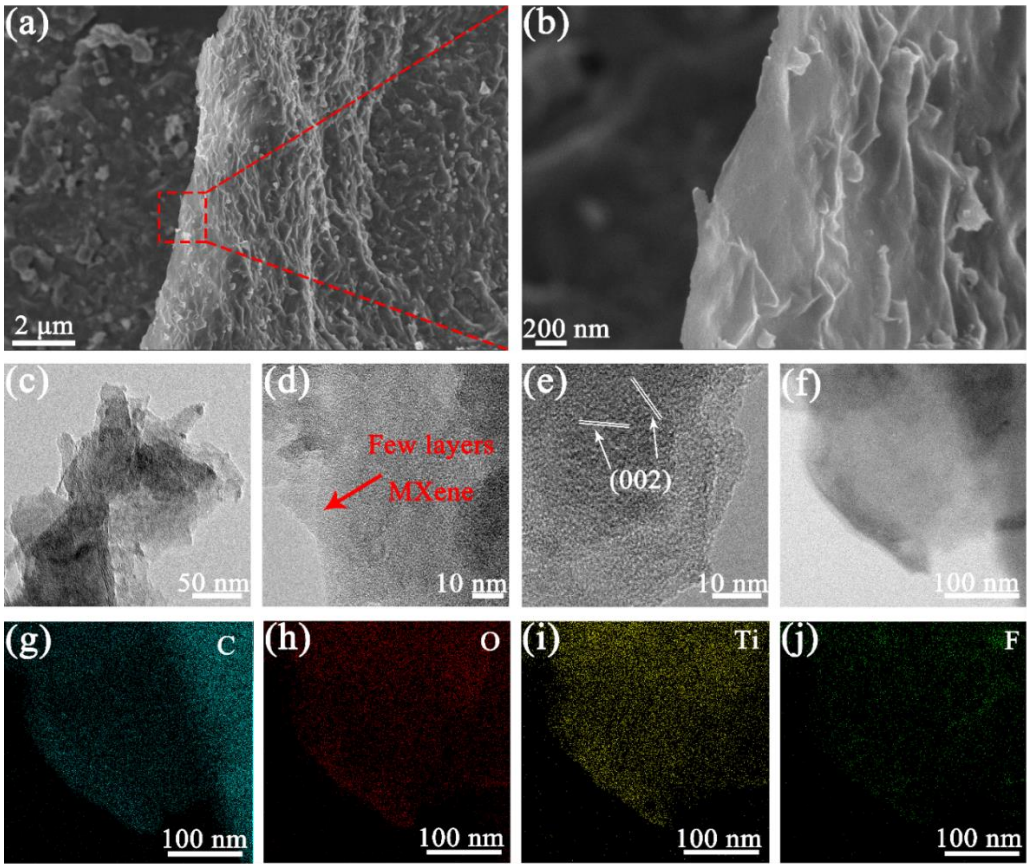

Fig. S2. SEM (a and b), TEM/HRTEM (c–e), and EDS elemental mapping images (f–j) of $Ti_3C_2T_x$ MXene.

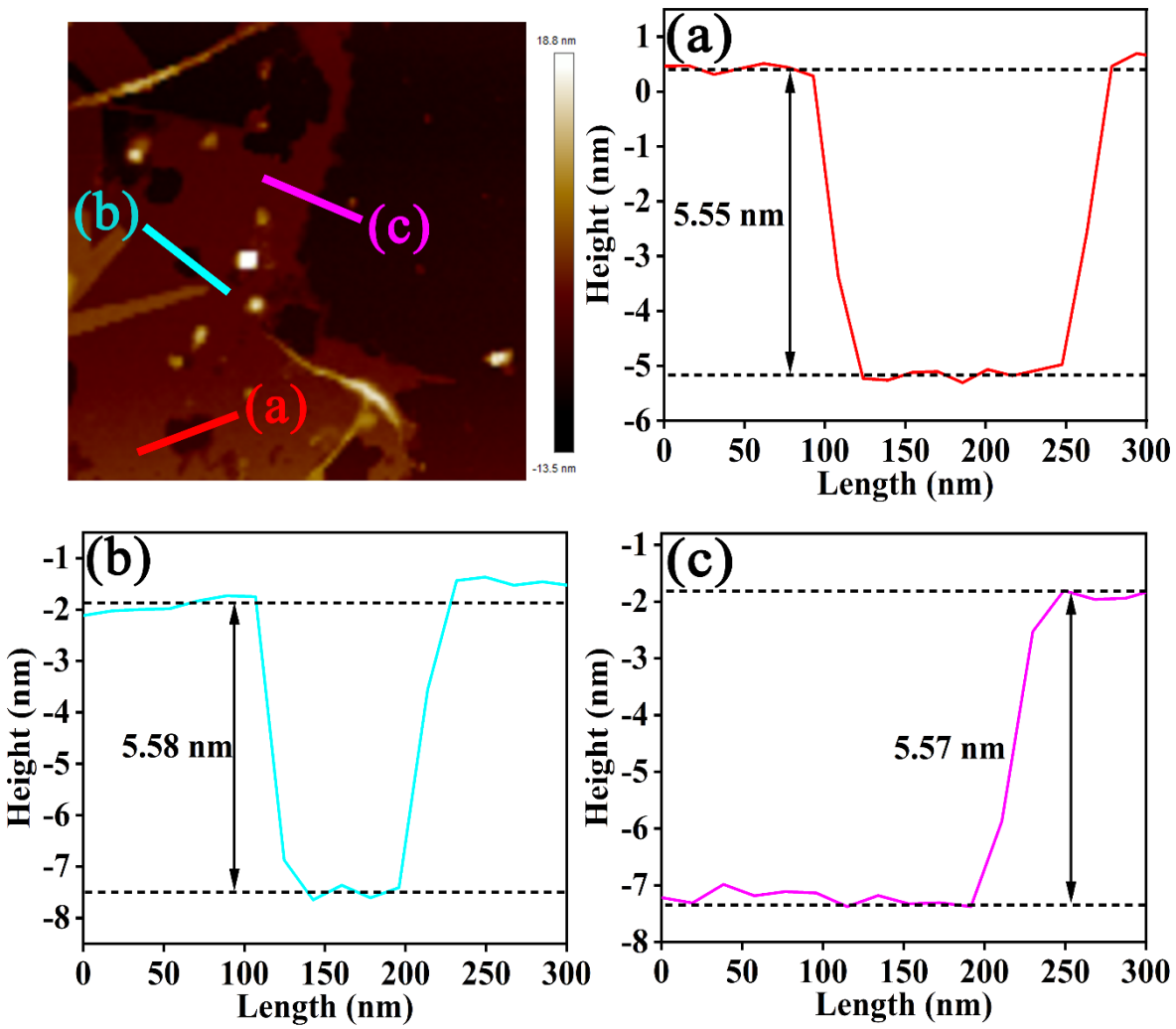

Fig. S3. AFM images and height profiles of $Ti_3C_2T_x$ MXene nanosheets.

Materials required for experimental synthesis

Oleylamine (OLA, 70%), Oleic acid (OA, 90%), Iron acetylacetonate($Fe(acac)_3$, ≥99.9%), 1-Octadecene (ODE,90%) were purchased from Sigma-Aldrich. $BiCl_3$ (99.97%) was purchased from Alfa Aesar. Ti_3AlC_2 (MAX phase) powder was purchased from Laizhou Kaixi Ceramic MaterialCo. Ltd. Hydrochloric acid (HCl) was supplied by Tianjin Tianli Chemical Reagent Co, Ltd. NOx gas (99.9%) was purchased from Dalian Date Gas Co.

Based on the experimental facts and the relevant literature [26], the possible involvement of $Fe(acac)_3$ in the reaction process is considered as follows:

(1) Production of primary free radicals

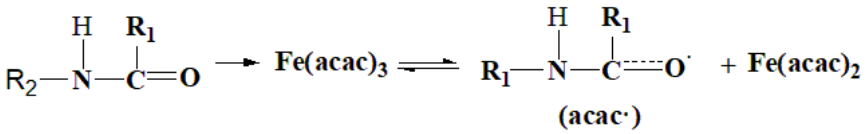

(2) The chain initiation

$$\mathbf{acac\cdot + Bi \rightarrow acac - Bi\cdot}$$

(3) The chain growth

$$\mathbf{acac - Bi\cdot + Bi \rightarrow acac - Bi_2\cdot}$$

$$\mathbf{acac - Bi_{(n-1)}\cdot + Bi \rightarrow acac - Bi_{(n)}\cdot}$$

(4) The chain termination

$$\mathbf{acac - Bi_{(n)}\cdot + Bi_{(n)}\cdot - acac \rightarrow acacBi_{(2n)} - acac}$$

During the reaction, $Fe(acac)_3$ acts as an initiator to first form reactive amide radicals, which form reactive monomeric amides with the metal atom Bi, and then assemble continuously with the monomer to promote chain growth. Finally, the growing active chains become inactivated and terminate the chains. Eventually, the terminated chains end to form independent nanocrystals.

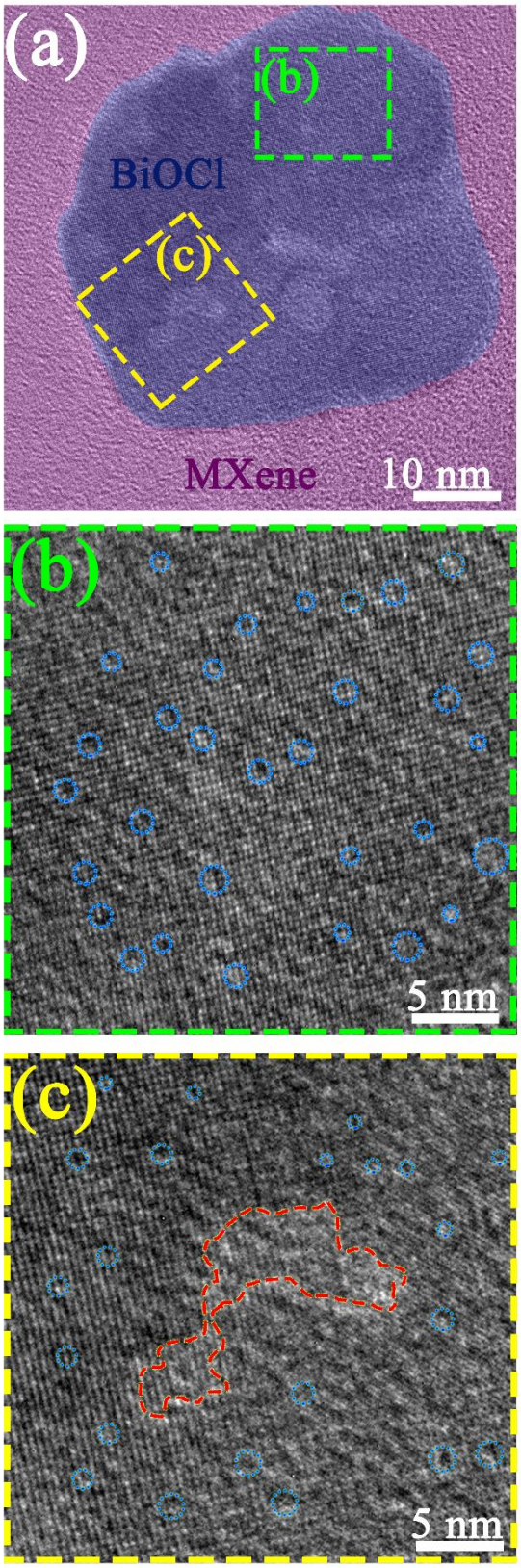

Fig. S4. (a-c) HRTEM images of BOM-3 (red lines show surface defects in BiOCl, light blue lines indicate point defects).

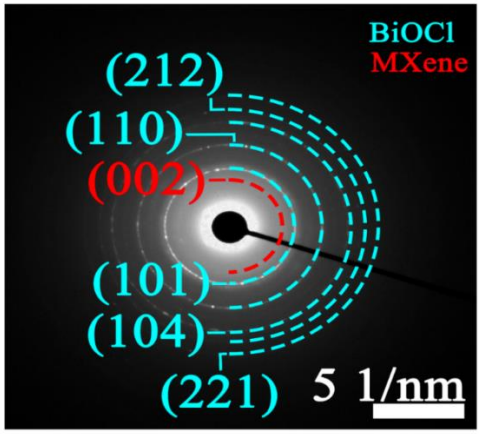

Fig. S5. SAED image of BOM-3 (blue lines show BiOCl, red lines indicate MXene).

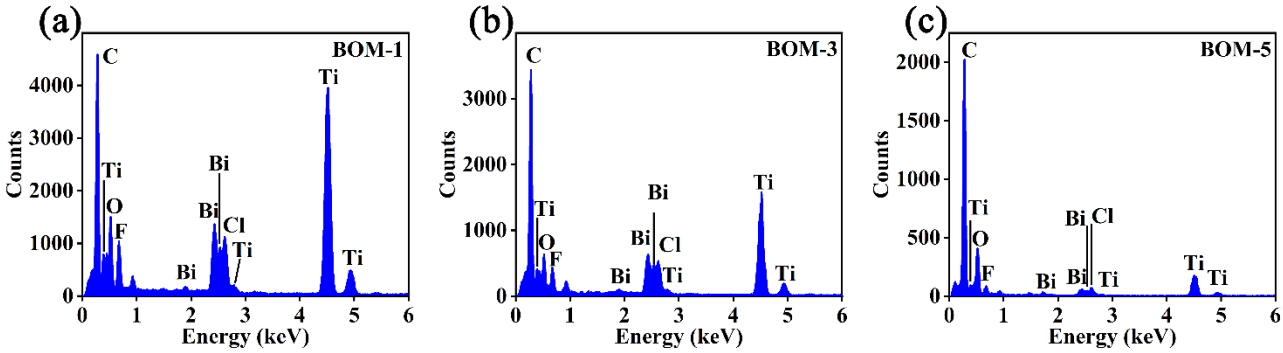

Fig. S6. TEM-EDS specture of BOM composites

Table S3 Summary of TEM-EDS results of BOM composites in terms of weight and atomic percentage.

Sample	Content	C	Ti	O	F	Bi	Cl
BOM-1	Wt%	38.5	22.4	5.8	3.1	26.0	4.2
	At%	72.2	10.5	8.1	3.6	2.8	2.8
BOM-3	Wt%	50.1	16.6	8.5	2.8	18.8	3.2
	At%	77.8	7.8	8.2	2.5	1.9	1.8
BOM-5	Wt%	79.6	4.6	9.6	0.9	4.4	0.9
	At%	89.4	1.3	8.1	0.6	0.3	0.3

Table S4 Parameters obtained by fitting an experimental curve to the equivalent circuit

Raw materials	R1 (Ω)	C1 (F)	R2 (Ω)	C2 (F)
BOM-1	8.286×10^{5}	9.204×10^{-12}	1.046×10^{5}	2.223×10^{-11}
BOM-3	1.801×10^{5}	1.728×10^{-11}	1.390×10^{4}	1.090×10^{-11}
BOM-5	2.219×10^{6}	9.775×10^{-12}	1.996×10^{5}	2.403×10^{-11}
V-BOM	3.135×10^{6}	9.545×10^{-12}	2.058×10^{5}	2.568×10^{-11}
BiOCl	6.167×10^{6}	6.568×10^{-10}	1.940×10^{6}	5.294×10^{-11}

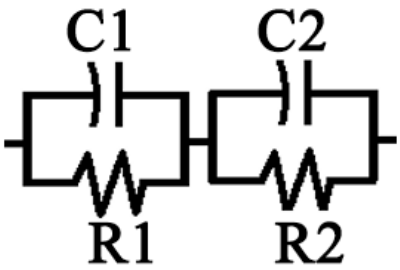

Fig. S7. The equivalent circuit model used to interpret the EIS data.

Table S5 Response, response time, and recovery time of BOM sensors at room temperature (RT=25 ℃, RH 25%).

Sample	**BOM-1**			**BOM-3**			**BOM-5**			**V-BOM**			**BiOCl**		
NO_2(ppm)	**S**	**T/s**	**Tr/s**	**S**	**T/s**	**Tr/s**	**S**	**T/s**	**Tr/s**	**S**	**T/s**	**Tr/s**	**S**	**T/s**	**Tr/s**
100	28.07	3.33	58.00	34.58	3.15	31.05	24.86	3.65	35.66	20.75	5.39	40.33	12.75	7.39	65.33
50	20.93	5.10	51.34	29.25	4.68	30.02	18.25	5.42	32.00	15.52	7.52	35.00	10.52	9.52	61.00
30	18.32	6.38	45.33	25.80	6.24	29.58	12.81	6.57	30.16	11.63	8.94	33.48	8.63	10.94	49.48
10	17.77	7.32	42.00	24.96	6.22	25.70	12.68	8.17	27.56	10.26	11.68	30.56	6.26	11.68	45.56
5	14.55	8.51	36.00	22.69	7.89	24.93	10.11	9.39	26.66	9.75	12.90	28.05	4.75	11.90	43.05
3	8.60	9.49	34.69	19.33	8.47	23.01	8.08	9.96	25.91	7.13	13.98	26.73	3.13	12.98	37.73
1	6.19	9.57	25.34	15.18	8.58	15.99	5.53	10.46	25.67	4.31	14.12	25.92	2.31	13.12	28.92
0.5	5.40	10.31	22.97	10.22	9.18	12.54	4.27	11.13	25.19	4.20	15.68	24.67	1.20	15.68	20.67
0.3	3.27	10.60	13.65	7.24	9.41	10.87	3.08	12.48	15.73	3.17	17.69	20.23	1.17	17.69	18.23
0.1	2.21	11.56	5.63	4.21	10.35	8.69	2.19	13.35	9.68	2.16	18.11	18.65	1.16	18.11	14.65
0.05	1.96	12.87	4.90	2.19	11.42	5.86	1.84	15.29	6.94	1.05	20.15	15.47	1.05	20.15	13.47
0.03	- -	- -	- -	1.02	12.68	3.63	- -	- -	--	--	--	--			

*S: Response T_s: Response time T_r: Recovery tim

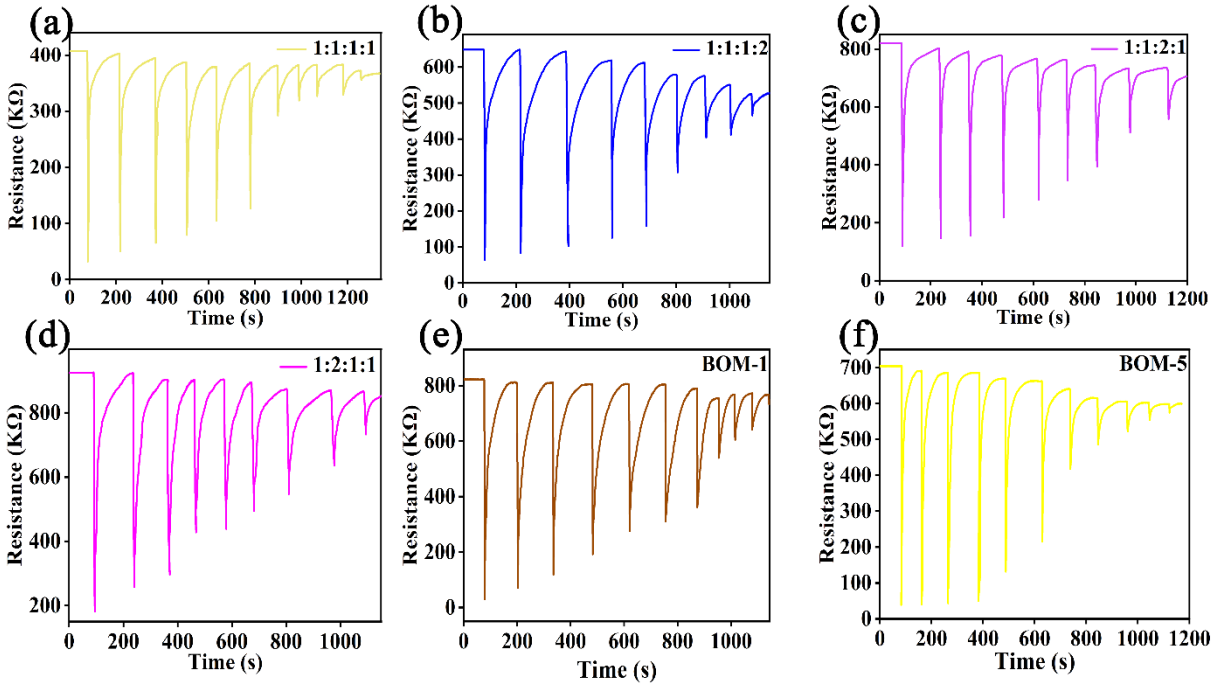

Fig. S8. Dynamic response-recovery time curves of the different ratios of $BiCl_3$: $Fe(acac)_3$: OA: OLA; (a)1:1:1:1; (b) 1:1:1:2; (c) 1:1:2:1 and (d) 1:2:1:1; Dynamic response-recovery time curves of the (e) BOM-1 and (f) BOM-5.

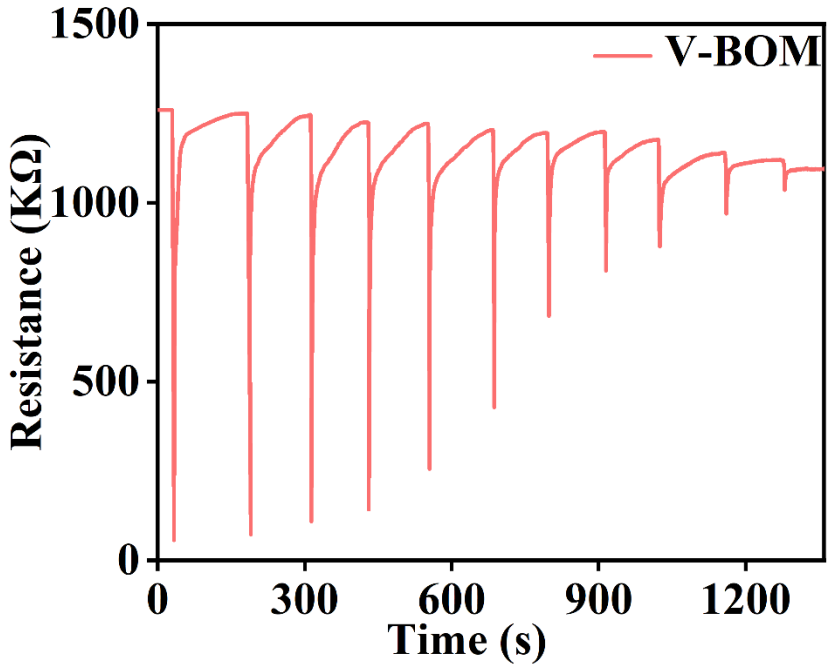

Fig. S9. Dynamic response-recovery time curves of the vertical growth of BOM gas sensors (V-BOM).

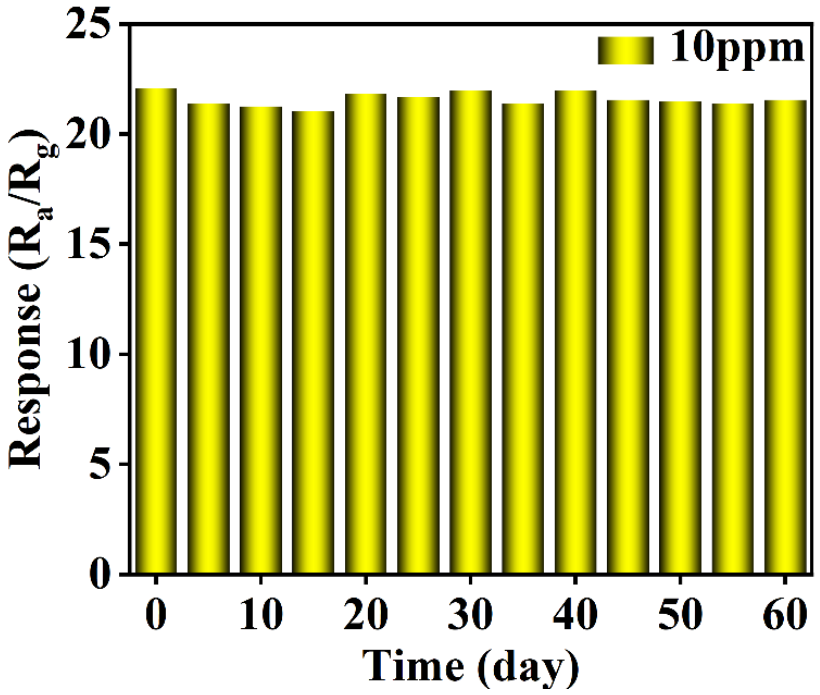

Fig. S10. Stability of BOM-3 sensor to 10 ppm NO_2 within 20 days (RH=80%)

Table S6 The response, response time and recovery time of samples at RH=80% for different NO_2.

Sample	BOM-1			BOM-3			BOM-5			V-BOM			BiOCl		
NO_2(pp)	S	T/s	Tr/s	S	T/s	Tr/s	S	T/s	Tr/s	S	T/s	Tr/s	S	T/s	Tr/s
100	22.07	5.78	39.65	30.54	5.58	35.08	20.35	5.98	42.36	18.38	6.10	45.33	2.56	6.39	55.00
50	20.35	7.25	38.24	28.38	6.21	34.88	18.55	7.39	41.00	16.32	7.49	42.00	2.45	7.52	47.00
30	19.68	7.83	37.96	23.26	7.35	30.25	17.30	8.38	39.51	11.89	8.58	40.48	1.87	8.94	41.00
10	18.88	8.24	32.42	22.08	7.89	27.68	15.64	9.00	35.00	10.97	9.35	38.56	1.56	9.98	33.54
5	17.69	9.36	30.58	18.54	8.34	26.38	13.19	10.59	32.08	9.64	11.25	35.05	1.37	10.56	31.09
3	12.55	10.22	26.68	13.24	9.40	20.35	10.73	11.94	28.00	7.35	13.98	30.73	1.19	15.98	22.00
1	8.39	11.37	20.37	9.76	9.89	15.37	6.51	13.12	26.07	4.88	14.28	28.92	1.13	18.12	15.00
0.5	4.36	12.36	15.53	5.44	10.25	11.72	4.33	15.00	20.00	4.15	17.88	22.67			
0.3	3.20	13.72	13.83	3.30	11.38	9.86	3.19	15.80	15.60	3.10	19.49	18.23			
0.1	1.06	14.20	8.69	1.14	12.84	8.56	1.02	16.00	10.76	1.16	20.61	15.65			
0.05				1.13	13.67	5.31									
										--	--	--			

***S: Response T: Response time T_r: Recovery time**

157 **Table S7** O 1s peak position and peak area ratio (%) of samples.

Sample	**BiOCl**			**BOM-3**			**BOM-3+NO_2**		
Peak	Chemisorbed oxygen	Oxygen vacancy	Lattice oxygen	Chemisorbed oxygen	Oxygen vacancy	Lattice oxygen	Chemisorbed oxygen	Oxygen vacancy	Lattice oxygen
Peak position(eV)	533.1	531.1	529.5	533.1	531.1	529.5	533.3	531.5	529.7
Peak area	463.5	1517.7	2102.9	491.6	2968.2	2823.7	148.5	4170.4	2157.6
Peak area ratio (%)	11.3	37.1	51.6	7.8	47.2	44.9	1.8	51.4	26.5
Sample	**BiOCl+NO_2**			**MXene**			**MXene+NO_2**		
Peak	Chemisorbed oxygen	Oxygen vacancy	Lattice oxygen	Chemisorbed oxygen	Oxygen vacancy	Lattice oxygen	Chemisorbed oxygen	Oxygen vacancy	Lattice oxygen
Peak position(eV)	533.5	531.9	530.0	532.5	530.3	529.3	532.9	531.5	529.6
Peak area	1002.8	3904.3	4829.3	3227.5	3467.6	3227.5	6763.1	9658.5	5680.1
Peak area ratio (%)	10.3	40.1	49.6	32.5	34.9	32.6	30.6	43.7	25.7

158 All the sensor was detected gas sensing under NO_2 for 1 h.

159

160

161

162

163

164

165

166

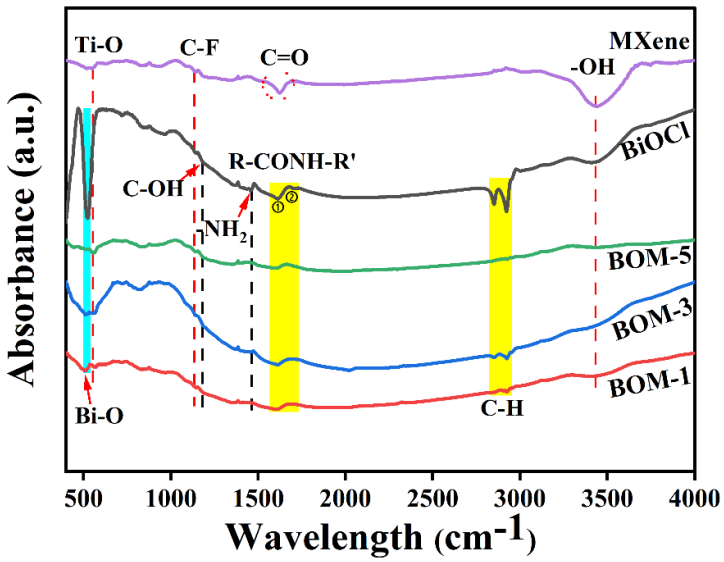

Fig. S11. FT-IR spectra of MXene, BiOCl, BOM-5, BOM-3 and BOM-1

The FTIR spectra (KBr) of MXene, BiOCl, and BOM nanocomposites are shown in Fig. S10. The spectra of MXene samples show peaks at 548 cm^{-1}, 1143 cm^{-1}, 1623 cm^{-1}, and 3443 cm^{-1}, which are attributed to Ti-O, C-F, C=O, and -OH stretching vibrations [27,28]. Compared to MXene, both BiOCl and BOM nanocomposites show a new band at 2852 and 2922 cm^{-1}, which may be caused by C-H bending in the alkyl chain [29]. Meanwhile, the intensity of the C-OH peak at 1181 cm^{-1} is rapidly increasing. A new band of Bi-O stretching vibration at 524 cm^{-1} can also be observed in BiOCl and BOM nanocomposites [30], which is a characteristic band of BiOCl. Also, the strong band at 1457 cm^{-1} is attributed to be caused by the vibrations of the $-NH_2$ group. This peak indicates that BiOCl and BOM nanocomposites are modified by organic groups of oleylamine [31]. Moreover, the peaks at 1612 cm^{-1} and 1717 cm^{-1} tend to be amide II (R-NHR', NH_2 deformation, N-H bending, and C-N stretching) and amide I (R-CONHR', C=O stretching), respectively. And the coexistence of these two peaks reveals the surface adhesion of O=C-NH species in BiOCl and BOM nanocomposites, which are N-oleoyl oleamide products resulting from the dehydration of oleic acid and oleylamine [32].

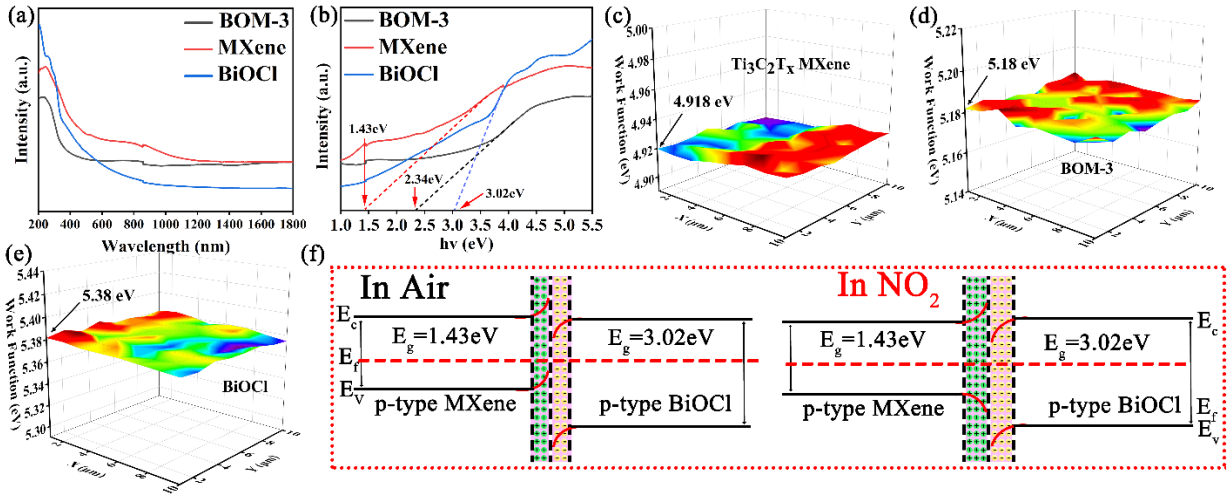

183

184 **Fig. S12.** (a-b) UV-vis diffuse reflectance spectra of BOM-3, Mxene, BiOCl; (c-e) Scheme of the

185 Kelvin probes of the $Ti_3C_2T_x$ MXene, BOM-3 and BiOCl; (f) Energy band structure of the BOM

186 composites in air and a NO_2 atmosphere.

187

188

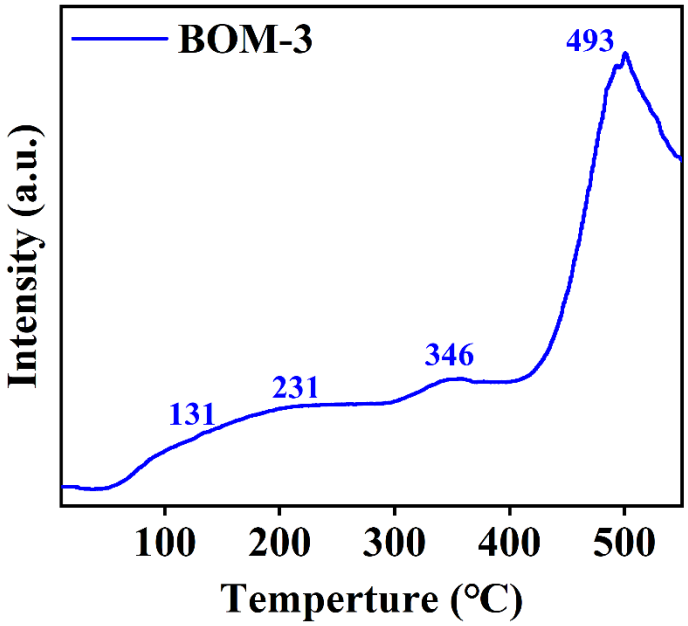

189

190 **Fig. S13.** NO_2-TPD of BOM-3 composite.

191

192

193

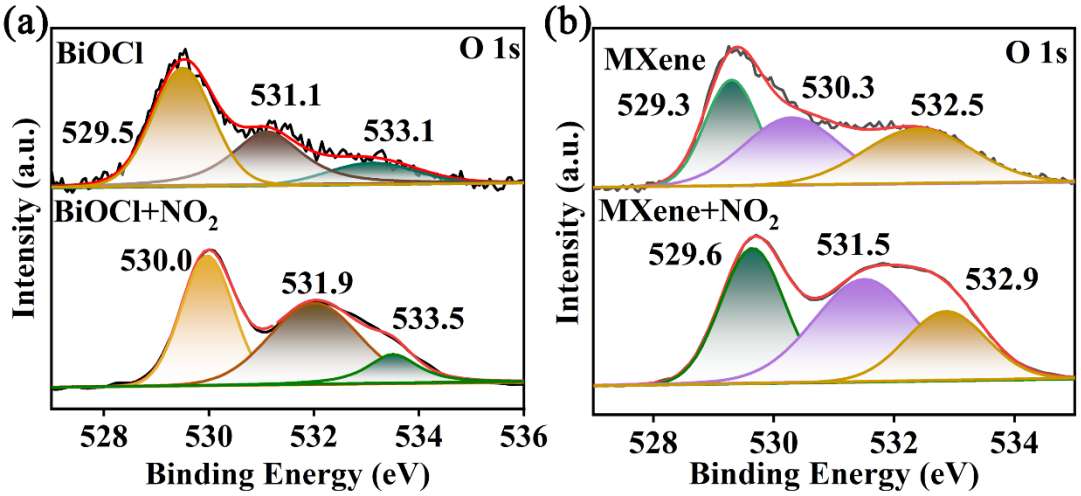

194

195 **Fig. S14.** O 1s XPS spectra of BiOCl and MXene without adsorbed NO_2 and after adsorption of NO_2

196

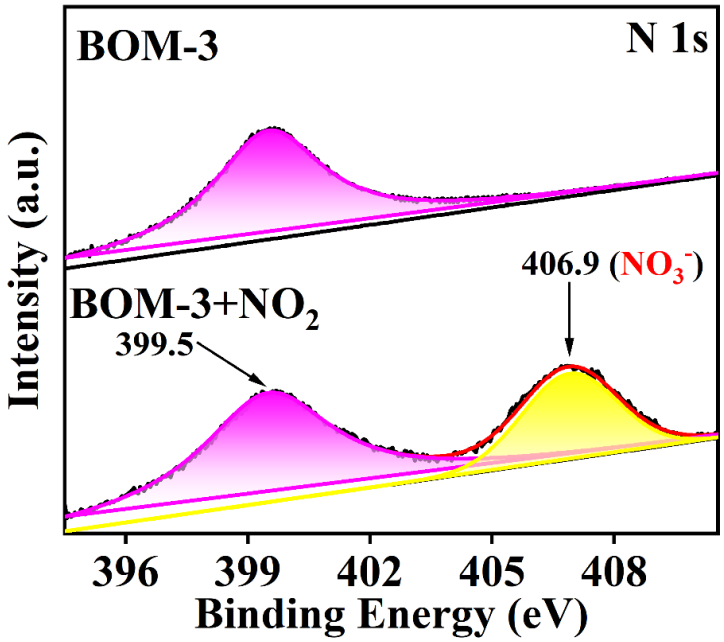

197

198 **Fig. S15.** N 1s XPS spectra of fresh and the BOM-3+NO_2.

199

200

201

202

203

204

205

206

207

References

1. C. R. Michel, N. L. López Contreras and A. H. Martínez-Preciado, Sensors and Actuators B: Chemical, 2012, **173**, 100-105.
2. C. R. Michel, N. L. L. Contreras and A. H. Martínez-Preciado, Sensors and Actuators B: Chemical, 2011, **160**, 271-277.
3. S. T. Navale, Z. Yang, C. Liu, A. Kumar, G. Sharma, P. Cao, V. B. Patil and F. J. Stadler, Journal of Alloys and Compounds, 2019, **778**, 532-541.
4. P. Velusamy, R. Xing, R. R. Babu, E. Elangovan, J. Viegas, S. Liu and M. Sridharan, Sensors and Actuators B: Chemical, 2019, **297**, 126718.
5. S. U. Mutkule, K. K. Tehare, S. K. Gore, K. C. Gunturu and R. S. Mane, Materials Research Bulletin, 2019, **115**, 150-158.
6. Z. Tao, Y. Li, B. Zhang, G. Sun, J. Cao and Y. Wang, Sensors and Actuators B: Chemical, 2020, **321**, 128623.
7. L. P. Chikhale, J. Y. Patil, F. I. Shaikh, A. V. Rajgure, R. C. Pawar, I. S. Mulla and S. S. Suryavanshi, Materials Science in Semiconductor Processing, 2014, **27**, 121-129.
8. R. Zhang, S. Y. Ma, J. L. Zhang, B. J. Wang and S. T. Pei, Journal of Alloys and Compounds, 2020, **828**, 154408.
9. S. Chakraborty and M. Pal, New Journal of Chemistry, 2018, **42**, 7188-7196.
10. W. Guo, Q. Zhou, J. Zhang, M. Fu, N. Radacsi and Y. Li, Sensors and Actuators B: Chemical, 2019, **299**, 126959.
11. Z. Ma, K. Yang, C. Xiao and L. Jia, J Hazard Mater, 2021, **416**, 126118.
12. J. H. Bang, M. S. Choi, A. Mirzaei, Y. J. Kwon, S. S. Kim, T. W. Kim and H. W. Kim, Sensors and Actuators B: Chemical, 2018, **274**, 356-369.
13. S. Gasso, M. K. Sohal and A. Mahajan, Sensors and Actuators B: Chemical, 2022, **357**,31427.
14. H. Yan, L. Chu, Z. Li, C. Sun, Y. Shi and J. Ma, Sensors and Actuators Reports, 2022, **4**, 100103.
15. Y. Zhang, Y. Jiang, Z. Duan, Q. Huang, Y. Wu, B. Liu, Q. Zhao, S. Wang, Z. Yuan and H. Tai, Sensors and Actuators B: Chemical, 2021, **344**, 130150.
16. Z. Yuan, Q. Zhao, Z. Duan, C. Xie, X. Duan, S. Li, Z. Ye, Y. Jiang and H. Tai, Sensors and Actuators B: Chemical, 2022, **363**, 131790.
17. J. Wu, Y. Liang, Z. Zhou, Z. Wu, H. Ding, W. Huang, K. Tao, W. Shi, B.-R. Yang and X. Xie, Sensors and Actuators B: Chemical, 2021, **344**, 130259.
18. H. Wang, M. Dai, Y. Li, J. Bai, Y. Liu, Y. Li, C. Wang, F. Liu and G. Lu, Sensors and Actuators B: Chemical, 2021, **329**, 129145.
19. C. Han, X. Li, Y. Liu, X. Li, C. Shao, J. Ri, J. Ma and Y. Liu, J Hazard Mater, 2021, **403**, 124093.
20. Q. Zhao, D. Sun, S. Wang, Z. Duan, Z. Yuan, G. Wei, J. Xu, H. Tai and Y. Jiang, ACS Sens, 2021, **6**, 2858−2867.
21. S. Gasso and A. Mahajan, ACS Sens. 2022, **7**, 2454−2464.
22. C. Fan, J. Shi, Y. Zhang, W. Quan, X. Chen, J. Yang, M. Zeng, Z. Zhou, Y. Su, H. Wei and Z. Yang, Nanoscale, 2022, **14**, 3441.
23. B. Zong, Qikun Xu, and Shun Mao. ACS Sens. 2022, 7, 1874−188.
24. Q. Xu, B. Zong, Y. Yang, Q. Li, S. Mao a,b, Sensors and Actuators B: Chemical, 2022, 373, 132696.
25. Qi. Xu, B. Zong, Q.Li, X. Fang, S. Mao, K. Ostrikov, J Hazard Mater, 2022, 424, 12749.
26. B. N. Misra, I. K. Mehta and D. S. Sood, Journal of Macromolecular Science: Part A - Chemistry, 2006, **14**, 1255-1268.
27. Y. Feng, H. Wang, J. Xu, X. Du, X. Cheng, Z. Du and H. Wang, J Hazard Mater, 2021, **416**, 125777.
28. B. Sun, H. Lv, Z. Liu, J. Wang, X. Bai, Y. Zhang, J. Chen, K. Kan and K. Shi, Journal of Materials Chemistry A, 2021, **9**, 6335-6344.
29. G. Qiu, T. Wang, X. Li, X. Tao and B. Li, Industrial & Engineering Chemistry Research, 2020, **59**, 11517-11526.
30. H. Wang, B. Liao, T. Lu, Y. Ai and G. Liu, J Hazard Mater, 2020, **385**, 121552.
31. J. Liu, L. Wang, J. Wang and L. Zhang, Materials Research Bulletin, 2013, **48**, 416-421.
32. M. H. Yang, S. S. Yuan, T. W. Chung, S. B. Jong, C. Y. Lu, W. C. Tsai, W. C. Chen, P. C. Lin, P. W. Chiang and Y. C. Tyan, Biomed Res Int, 2014, **2014**, 209469.